Measurement of Losses in Dry-Type Air-Core Reactors Using Infrared Thermography

DENISON GIMENES MESQUITA[1] (Student Member, IEEE),
EDSON DA COSTA BORTONI [1] (Senior Member, IEEE),
DAVI MARCELO FÉBBA[1] (Student Member, IEEE),
AND ROBERTO TEIXEIRA SINISCALCHI[2] (Senior Member, IEEE)

[1]Electric and Energy Systems Institute, Itajubá Federal University, Itajubá, Minas Gerais 37501-903, Brazil
[2]Minas Production Department, Furnas Centrais Eletricas, São José da Barra, Minas Gerais 37945-000, Brazil

CORRESPONDING AUTHOR: E. C. BORTONI (bortoni@unifei.edu.br)

ABSTRACT This paper aims to present a technique to estimate the losses of a dry-type air-core reactor (DTACR) assembled with one cylinder based on calorimetry principles while employing infrared thermography techniques. The technique is intuitive, practical, and easy to apply both in a laboratory and in the field. Nowadays, the losses on DTACR can be measured only inside of specific laboratories and the equipment shall be disconnected from system and powered-off. Instead of installing contact temperature sensors in the reactor's internal and external surfaces, temperature measurements were remotely performed with equipment in regular operation and the losses can be obtained by the method proposed. The paper presents the nature of the losses and the theoretical basis of the proposed method. The results obtained from the proposed technique are compared to those achieved by the standard method and used to calculate results through tests performed on prototypes.

INDEX TERMS Dry-type air-core reactor (DTACR), infrared thermography, total loss determination.

NOMENCLATURE

A	Surface area (m^2)
β	Coefficient of volumetric air expansion (°C^{-1}).
D	Diameter of the reactor (m).
f	Fundamental frequency (Hz).
g	Gravity acceleration (m/s^2).
G_r	Grashoff number.
h'	Heat transfer coefficient (W/m^2°C).
$\dot{I}_i$	Current in each layer (A).
k	Thermal conductivity of the air (W/m°C).
L	Length of the reactor (m).
L_{ii}	Self-inductance (H).
M_{ij}	Mutual inductance between layers (H).
P	Convection and irradiation loss (W).
P_r	Prandtl number.
R_i	Layer resistance (Ω).
T_a	Ambient temperature (°C).
T_s	Surface temperature (°C).
$\dot{U}$	Voltage over the reactor (V).
v	Kinematic viscosity of air (m^2/s).
Γ	Geometry Number.

I. INTRODUCTION

DRY-TYPE air-core reactors (DTACR) are among the most critical pieces of equipment in high voltage transmission and distribution systems and industrial systems as long as they can be installed at any voltage level. The technology type of reactor applied for several applications has changed over the years based on the project evolution. Advances in the construction and new materials improved mechanical features that allow the reactors to withstand higher fault currents. The applications of DTACR extend into current limiting, phase reactors, bus-tie reactors, neutral-grounding, arc-suppression, inrush limiters for capacitor banks, power flow control, shunt reactors; thyristor-controlled reactors, harmonic filter, reactors for HVDC application, and arc furnace reactors [1]–[6].

Many researchers are concerned with developing predictive methods that can evaluate the equipment conditions in real-time without disconnecting from the power network [7]–[10], increasing energy efficiency while avoiding undesired energy losses [11]–[13]. It is increasingly needed to develop studies related to the diagnosis of failures in DTACR and the techniques used to progressively improve [14], 15].
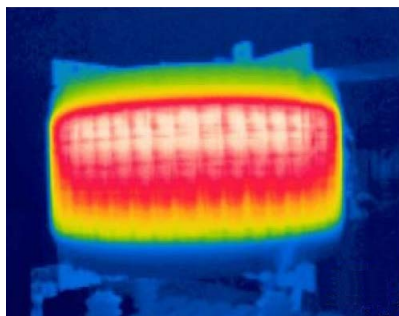
FIGURE 1. DTACR infrared image.

FIGURE 2. Design details of the DTACR.

With the constant expansion of electric systems, concessionaires are continually seeking improvement and new techniques to optimize energy transmission and distribution [17], [18]. On the other hand, the reactor manufacturers have the challenge of technically meeting the customer specification by offering their most economical solution [19], [20]. In addition to the previous points, the theoretical losses versus field losses, the monitoring of the reactor's life cycle, and the equipment's operating conditions can be evaluated by dissipated electrical losses in monitoring and working temperature.

The DTACR is a piece of equipment that has relatively simple construction characteristics [21]–[24]. The conductor is insulated through an insulation film helically wound in the technology studied here, and the conductors are mechanically immobilized through encapsulation of fiberglass filaments impregnated with epoxy resin. One or more layers of conductors may be connected in parallel resulting in one or more cylinders. The load losses associated with a DTACR are composed of winding current loss, induced current loss in the wires, and Foucault loss due to flux linkage in the metal closure [24]–[28].

The main concentration of losses during the operation is located in the windings. Cost considerations related to losses are of fundamental importance in defining both the equipment design and DTACR, the routine measurements during manufacturing.

Methods to measure the wire losses are described by the most prevalent standards [29]–[32]. In the constant quest for new losses measuring techniques, some recent works have already proved the infrared (IR) thermography's effectiveness for loss determination on small motors in a laboratory [33]–[35]. Theoretical models used to study the synchronous machine losses have been using the same method developed, showing favorable agreement with test results [36]–[38].

In the face of the presented constraints, the use of IR thermography to measure the DTACR losses is welcome. The thermography technique is based on the principle that all of the losses are converted into heat, a reasonable approach. Beyond that, the reactor surface is quite regular and well measured. Figure 1 shows an infrared image of an ACR.

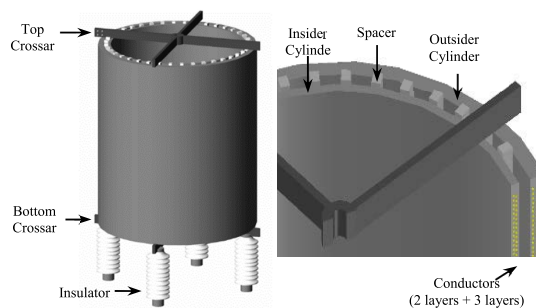Therefore, three single-cylinder DTACR prototypes were constructed with features similar to the equipment used in the field. The main difference between the prototypes was the number of aluminum layers inside of a single-cylinder. Standard tests were applied to measure each prototype's total losses, including measurements with the proposed technique, for comparison purposes.

Seeking high accuracy, the obtained data for thermography analysis considered all of the influential factors regarding the measurements, view angle, wind speed, emissivity, voltage drop, ambient air temperature, and the current flowing through the ACR. Statistical methods were applied to define how many images along the ACR periphery would be necessary in order to achieve the highest accuracy.

A brief report was prepared for each sample with all of the data collected and diagnosis. The reference measurements were established in the next step. Therefore, this work exhibits the applicability, methodology, equipment required, and the precautions to obtain the best method response.

IR thermography has proven to be a valuable tool for finding hot spots, the electrical system sub-size, equipment overloading, and imbalance between the phase wires; now, it has also proven to be a reliable tool for evaluating losses DTACR.

Therefore, this proposal aims to present a technique for measuring the total losses of a DTACR with single-cylinder using infrared thermography to allow measurements in challenging access environments at high voltage levels. This work also seeks to develop a first-step procedure for both manufacturer and concessionary to identify losses on dry-type ACR with single-coil through infrared thermal images in a straightforward, accurate, and easy way.

II. THE AIR-CORE REACTOR

DTACR occupies about 45% of the area required to install an oil-filled reactor, present low operational costs, do not use maintenance, and protect instruments typical of reactors with insulating liquid. Additionally, they have no explosion risk, withstand strong overloads and excellent resistance to short-circuit due to the configuration and construction of coils, and allow a temperature rise above isolated oil reactor.

The fully encapsulated with solid dielectric DTACR is employed across the entire voltage range, from distribution voltage level to high and extra-high voltage levels. Modern DTACR has been manufactured with windings fully

encapsulated through insulations made of laminated films, Kraft paper, fiberglass, and enamel dielectric, among others.

As in all electrical system equipment, the DTACR also has electrical losses when energized. Electrical losses emerge as the reactor operation's main cost, mainly due to the low operational and maintenance costs. Based on this aspect, understanding the primary phenomenon that causes losses and developing an accurate system to know these phenomena in the equipment becomes of utmost importance. Therefore, design and losses are discussed as follows.

A. DTACR DESIGN

Different design metrics can be chosen for the DTACR design. However, the most common configuration is the cylindrical shape as it is the most appropriate for standard manufacturing methods, as shown in Fig. 2. The active part of the reactor is composed of encapsulated parallel coaxial, copper or aluminum, coils. Its assembly consists of one or more cylinders built by coil layers winding over each other.

The electromagnetic coupling between turns results in self and mutual inductances which affects the equipment's inductance.

Between the cylinders, there are cooling paths supported by sustaining bars manufactured using an insulating material. The cross arms are an aluminum-made structure located on the top and bottom of the reactor, operating as connecting bridges between the terminals and the system. They play an essential role in the current distribution between the wire layers and act as a supporting structure responsible for guaranteeing that the reactor remains at a ground distance.

A single-layer circular reactor, built with a single helical winding of a single wire over a cylindrical mandrel, has basic construction geometry found in several electrical windings. The single-layer circular coil has a simple concept, low manufacturing cost, and low effective winding capacitance, among other advantages.

B. DTACR DESIGN

According to the equivalent circuit of Fig. 3, the most general equation relates applied voltage, currents, inductances, and self-inductances in concentric and non-concentric coils, is:

$$
\left[
\begin{bmatrix}
R_1 & 0 & \dots & 0 \\
0 & R_2 & \dots & 0 \\
\vdots & \vdots & \dots & \vdots \\
0 & 0 & \cdots & R_i
\end{bmatrix}
+ j2\pi f
\begin{bmatrix}
L_{1,1} & M_{1,2} & \dots & M_{1,i} \\
M_{2,1} & L_{2,2} & \dots & M_{2,i} \\
\vdots & \vdots & \dots & \vdots \\
M_{i,1} & M_{i,2} & \cdots & L_{i,i}
\end{bmatrix}
\right]
\begin{bmatrix}
\dot{I}_1 \\
\dot{I}_2 \\
\vdots \\
\dot{I}_i
\end{bmatrix}
=
\begin{bmatrix}
\dot{U} \\
\dot{U} \\
\vdots \\
\dot{U}
\end{bmatrix}
\tag{1}
$$

The inductance estimation of a single layer coil is based on a cylindrical current wire equation, i.e., a winding in which the current flows around the axis of a cylinder in a layer
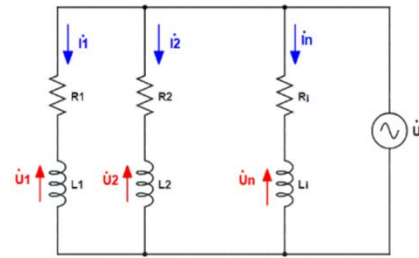

FIGURE 3. Equivalent circuit of a DTACR.

of infinite radial thickness the surface of this cylinder. The calculation method starts with a Neumann expression that is a direct Biot-Savart Law application [39].

A conductor's resistance is directly proportional to its length and resistivity and inversely proportional to its section's area. With the average diameter of each layer, the DC resistances at a specific reference temperature are determined and the calculation of the current distribution in the reactor is possible.

III. THE AIR-CORE REACTOR LOSSES

The average temperature in a DTACR under rated voltage and current conditions is a function of the total losses. Such losses are due to the winding itself and induced in other metallic structural components close to the reactor. The losses are divided into four main groups.

A. CURRENT LOSSES

This type of loss is the most significant. It happens in the conductors and is proportional to its resistance and to the squared flowing current, resulting in temperature rise and releasing heat in the reactor structure. Such losses are of simple calculation at fundamental frequency.

B. SKIN EFFECT LOSSES

This is a natural current loss that happens when the apparent resistance of an electrical conductor is greater than the DC resistance due to the skin effect. This increase of resistance is proportional to the frequency's square root, resulting in a proportional loss increase.

C. PROXIMITY EFFECT LOSSES

When two or more conductors are placed close together, the electromagnetic fields interact with each other, generating eddy currents in the adjacent conductor. The result is a high current density concentrated in that part of the wire farthest from the interfering conductor, increasing the apparent resistance of adjacent conductors and in the current loss as well, causing undesirable heating.

D. EDDY CURRENT LOSSES

Eddy currents are closed loops of induced current that circulate in planes perpendicular to the magnetic flux. The absence of a magnetic core concentrate in the field results in flux inside and around the DTACR. The dispersed field

induces eddy currents in the reactor parts, such as windings, crossarms, corona rings, supports, terminals, connectors, busbars, and any adjacent electrically conductive material, causing current losses. For DTACR with small dimensions, the eddy current losses are small compared to the winding losses, which is why they are disregarded.

IV. THE CALORIMETRIC METHOD

The calorimetric method, or thermodynamic method, combined with infrared thermography techniques, has already been widely used to determine losses in many electrical machines with outstanding results [33]–[38]. The technique applied is based on determining the total loss by measuring the temperature of the external surface.

It is assumed that all the losses are converted into heat. The heat created by the total loss in a DTACR is dissipated by mechanisms of convection and radiation, as long as the conduction transfer is minimal, in which case is often disregarded. On the other hand, convection is classified into natural convection, which dissipates heat into the environment naturally. Likewise, forced convection dissipates heat through fans. Except for rare cases, natural convection, compared to forced convection, is the most crucial process for cooling DTACR. Losses due to natural convection and irradiation appear when the reactor's active part is in contact with ambient air and is given by [40].

$$P = h'A\,(T_s - T_a) \tag{2}$$

The application of (2) and the usage of infrared thermography techniques, image processing, and ambient temperature measurement turn the process into an interesting process to estimate the total losses in DTACR with a single coil.

The average surface temperature is determined using IR thermography images, while the ambient temperature is obtained using regular sensors.

The heat transfer coefficient is fundamental to the accuracy of the proposal. It is difficult to obtain since convection and radiation in vertical walls are complex phenomena [40]. For some systems, an analytical calculation is possible, while for other more complex situations the determination of this parameter may be either experimental or based on numerical methods [41]. However, this parameter is dependent on the refrigerant fluid characteristics and, for the air, can be described by the following equation.

$$h' = \frac{k\,\Gamma\,(G_r P_r)^{0.25}}{L} \tag{3}$$

While Prandtl number is 0.7 for air, Grashof number is:

$$Gr = \frac{g\beta\,(T_s - T_a)\,L^3}{v^2} \tag{4}$$

Considering the cylindrical shape of a DTACR, the heat transfer coefficient is also subject to its dimensions. The geometry coefficient is empirically obtained and relates the parameter heat transfer coefficient's dependence
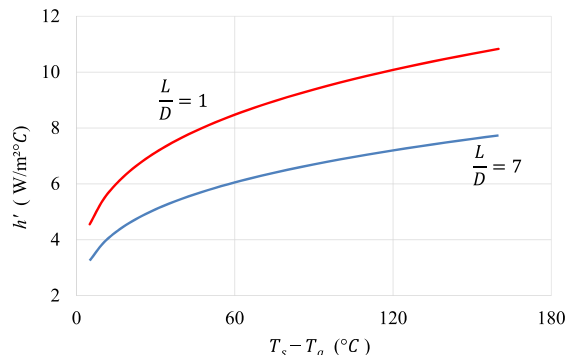

FIGURE 4. Influence of surface and ambient temperatures difference over the heat transfer coefficient for different length per diameter ratios.

TABLE 1. Input and output design parameters of the DTACR prototypes.

Quantity	Prototype 1	Prototype 2	Prototype 3
INPUT			
Inductance (H)	1.461	1.464	1.472
Rated Current (A)	25.80	36.87	45.38
Frequency (Hz)	60	60	60
Inner Diameter (mm)	251	250	249
Ambient Temperature (°C)	23.7	21.2	22.2
OUTPUT			
Number of Turns	90	92-89	94-90-89
Height (mm)	242	247	254
Diameter (average) (mm)	255	257	258
Inner and Outer Fiber (mm)	1	1	1
Average Temperature (°C)	101.5	99.0	100.1
Calculated Total Losses (W)	339.9	348.1	356.5

with the diameter and the height of the equipment, according to (5), when L/D ratio is less than ten [42].

$$\Gamma = L^{0.25}\left[3.017 + 1.25 10^{-1}\left(\frac{L}{D}\right) - 14.58 10^{-2}\left(\frac{L}{D}\right)^2\right.$$
$$+ 61.39 10^{-3}\left(\frac{L}{D}\right)^3 - 13.55 10^{-3}\left(\frac{L}{D}\right)^4$$
$$\left. + 1.34 10^{-3}\left(\frac{L}{D}\right)^5 - 4.76 10^{-5}\left(\frac{L}{D}\right)^6\right] \tag{5}$$

Figure 4 shows the variation of the heat transfer coefficient for several temperature differences.

V. PROTOTYPES DESIGN AND MEASUREMENTS

In order to verify the calorimetric method applicability for measuring the total losses of DTACR, three small scale prototypes with similar features of reactors that were applied in the field were constructed. Proprietary software for DTACR design and parameters calculation according to fabrication data was used. An example of its application is shown in Fig. 5.

Table 1 shows the input data and the main results of the software application. The main difference between the prototypes is the number of layers, which aims to verify
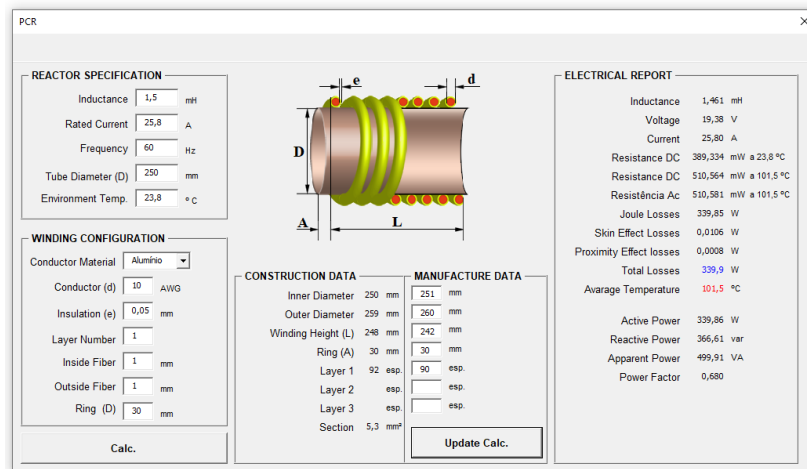
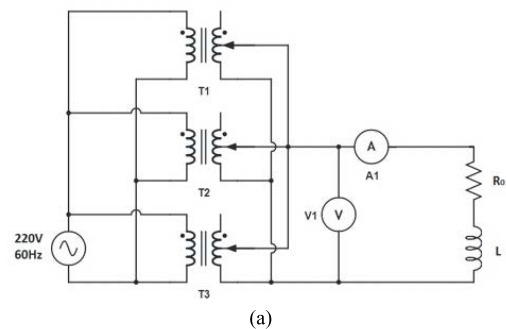**FIGURE 5. Example of application with input and constructive data, manufacture information, and design report.**

FIGURE 6. Developed prototype aspect. Three prototypes were developed with different number of layers each one.

FIGURE 7. Electrical testing diagram (a) and laboratory setup (b).

TABLE 2. Quantities measured by the end of the temperature rise tests.

Prototype	Voltage (V)	Current (A)	Power (W)	Inductance (H)
1	19.327	25.80	342.9	1.44
2	22.470	36.87	351.4	1.46
3	26.290	45.38	358.0	1.47

the behavior of the proposed method in facing of different design specifications. In all cases, the conductor material is aluminum, 10 AWG, and has an insulation width of 0.05 mm.

The final aspect of prototypes is shown in Fig. 6. For fundamental frequency and small and medium-sized reactors, the losses in the crossarms, used for connecting the windings to the terminals, have small participation in the total losses. These losses rarely exceed 0.5% of the total losses released in a piece of equipment. Therefore, the prototypes were assembled without crossarms, which does not affect the object of the work.

The calorimetric method associated with infrared thermography techniques consists of measuring the total losses of the DTACR under rated current. The application may be considered as a temperature rise test, or a type-test, as described in the standard IEC-60076-6 [29] and used to investigate the proposed methodology.

The temperature-rise test's primary purpose is to verify the reactor's final temperature based on the injection of the design rated current. It aims to reproduce the electrical conditions as close as possible to which the reactor would be subjected. Therefore, the temperature rise test is the primary

basis for comparing the real losses and those obtained by the proposed technique.

FLIR E40 is the thermal camera to be used, and, before the temperature rise test, it is necessary to perform its calibration. The reflected radiation temperature was adjusted using the Lambert radiator method with crumpled aluminum foil [43].
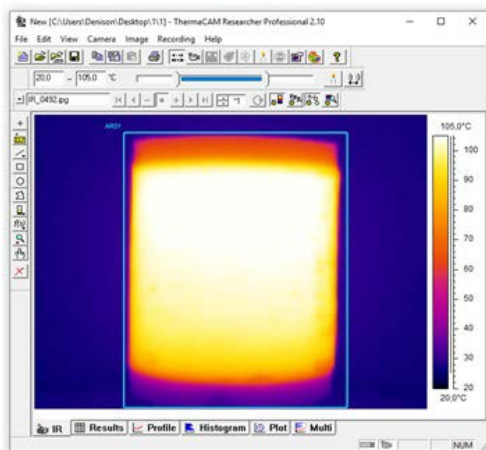
FIGURE 8. Area selection of infrared thermal image.

TABLE 3. Average temperature of each IR thermal image.

Image	Prototype 1 (°C)	Prototype 2 (°C)	Prototype 3 (°C)
1	102.0	100.3	100.7
2	101.6	100.4	100.5
3	101.2	100.0	100.5
4	101.1	99.6	100.6
5	101.3	100.0	100.6
6	101.5	99.6	100.4
7	101.5	99.4	100.3
8	101.8	99.7	101.0
9	101.5	99.8	100.9
10	100.8	99.6	100.6
11	100.9	99.2	100.3
12	102.1	99.3	100.4

The emissivity was adjusted by comparing the readings of the thermo-camera to a contact temperature detector, reaching 0.90. The distance between the camera and the prototype was one meter. The camera was positioned perpendicularly to the object and must obey a maximum angle of 50° according to [44]. The ambient temperature throughout the test was monitored and the test circuit system is shown in Fig. 7. Few seconds before ending the test of each prototype reactor, measurements of inductance and total losses were performed using the power analyzer Voltech PM300. Table 2 shows the total loss is the measured power which is used as a reference when evaluating the proposed technique.

VI. CALORIMETRIC METHOD APPLICATION

If on the one hand errors associated with thermal imagery temperature measurement must be minimized, on the other hand, it is known from research results that the viewing angles of the infrared waves emitted by the radiant body can introduce errors and compromise the measurement [44], [45]. Due to the reactors' cylindrical shape and reduced measurement errors, only a portion of the outer surface area measurements was considered. Therefore, images of the reactor surface were taken at every 30° of rotation, resulting in twelve thermal images covering the reactor's full surface.

Electrical and physical access restrictions avoided internal images of the reactor to be recorded. Given the restrictions,
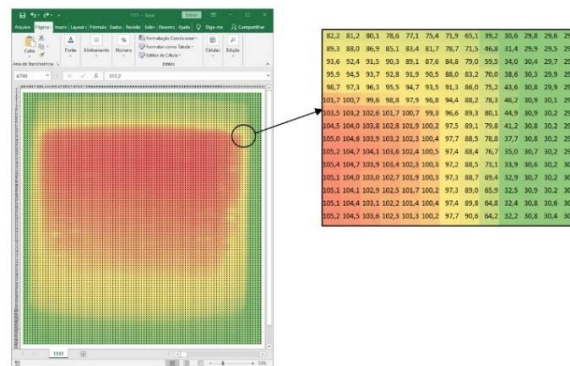

FIGURE 9. Pixel matrix of the infrared thermo image.

internal and external points with the same coordinates are considered to have the same temperature.

Infrared thermal images were processed using the ThermaCAM Researcher Pro 2.10 software. This software allows for selecting parts of the infrared image with the function 'polygon' and the function' box area,' as shown in Fig. 8. It is also possible to transform the image into a matrix by saving the image selection as a '.csv' file that is eventually read by a spreadsheet. Each cell of the spreadsheet represents a pixel of the FPA array with an associated temperature. The resultant pixel matrix is presented in Fig. 9. The influence of the target angle in the temperature measurement can be seen in Fig. 10. For the horizontal line drawn in the pixel matrix shown in Fig. 10 (a), the temperature is shown in Fig. 10 (b).

It was expected to have an approximately constant temperature for the same height line instead of the observed temperature decay. This is due to the emissivity variation of inclined planes. For example, an object can be seen beyond a window in a perpendicular viewing. Nevertheless, the glass window acts as a mirror for small angles.

It can be seen that measurements for viewing angles greater than 50° from the centerline overload the results with considerable errors that can exceed 2% of the reading value, which is consistent with a previous study [45]. Thus, it is usual to consider the optimum area covering angles between −30° to +30° from the centerline, as in Fig. 11.

From each of the twelve captured images, the pixel matrix generates three thousand temperature measurement data. Due to the non-homogeneous temperature setting on the reactor surface, the Anderson-Darling normality test applied to the data sample demonstrated that it does not follow a normal standard distribution [46]. Thus, only the average temperature of each of the twelve thermal images collected are presented in Table 3. In applying a statistical, computational tool to perform the analysis on average temperatures in Table 3, the information available in Fig. 12 to Fig. 14 for the three prototypes is shown.

By classifying the data series in a histogram and performing the normality test, it is possible to verify that the average temperatures meet the normality test's assumption and confirm the Gaussian distribution. This result makes it possible to analyze the data in a probabilistic way.
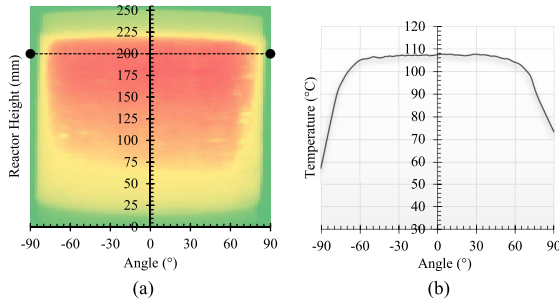
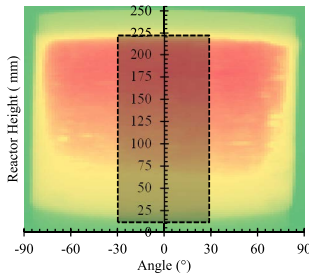**FIGURE 10.** Target angle influence on temperature measurement.

FIGURE 11. Useful area of IR thermograph image.

TABLE 4. Average temperature of all IR thermal images.

Prototype 1 (°C)	Prototype 2 (°C)	Prototype 3 (°C)
101.4	99.7	100.6

TABLE 5. Total losses calculated by calorimetric method.

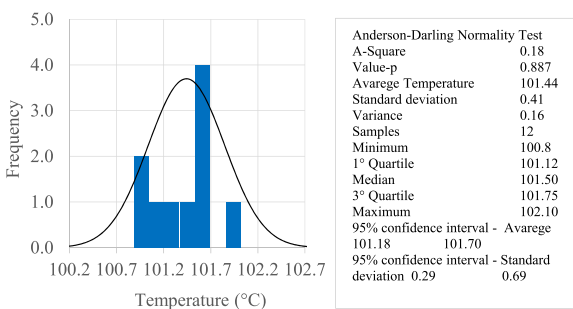| Quantity	Prototype 1	Prototype 2	Prototype 3
Surface area (m²)	0.4944	0.5006	0.5100
Ambient temperature (°C)	23.7	21.2	22.1
Surface temperature (°C)	101.4	99.7	100.6
Total losses (W)	346.6	355.6	362.2

FIGURE 12. Normality test, Prototype 1.

Each standard curve provides the prototype's average temperature, standard deviation, variance, and confidence intervals. A brief inspection of the histogram elements within the density and probability function curve shows a fair disposition of the elements, which characterizes the absence of abnormal points and with intrinsic errors that must be discarded. Also, small values of variance, such as those found in the graphs, indicate a low dispersion of the elements compared to the average. The prototypes' average temperatures are identified according to the averages resulting from the previous analysis. The values are given in Table 4.
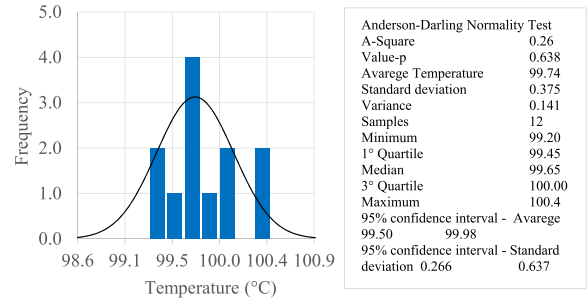

FIGURE 13. Normality test, Prototype 2.

TABLE 6. Total losses compariso.

Quantity	Prototype 1	Prototype 2	Prototype 3
Calculated Losses (W)	339.86	348.09	356.55
Measured Losses (W)	342.9	351.4	358.0
IR Thermography (W)	346.6	355.6	362.2

The knowledge of the surface area exposed to convection is critical in calculating the losses of a reactor using the infrared thermography technique. The obtention of this area is relatively simple in the case of the DTACR with a cylindrical shape. The reactors with a single-cylinder, the basis of this study, have the internal and external surface well defined. With the internal and external diameter and the height of the active part of the equipment, the total area exposed to convection is then obtained. Finally, the heat transfer coefficient is obtained from (3) the resulting 9.0. All components necessary for calculating the total losses in the DTACR prototypes are available for being utilized (2).

Table 5 shows these variables and the total loss calculation for each prototype, using the infrared thermography techniques. The results obtained from this technique, the calculations obtained from the design software, and the total loss measurements according to the standard IEC-60076-6 [29] are placed in Table 6 for comparison purposes.

The difference between the three values is minimal and maintains the same proportion, i.e., the value obtained from the infrared thermography techniques is always greater than that obtained from standard measurements and more significant than the design's value. The small differences corroborate with the proposed simplifying approaches to make the infrared thermography techniques feasible. It is also identified that a single-coil DTACR, which may differ in its number of layers (from 1 to 3), implies no significant influence on the measured losses, showing that the proposed method is suitable even when there is more than one layer in the DTACR.

The values of losses found with the proposed technique are close to the reference values since the variations are less than 1.5%. For applications previously defined, the results were extremely satisfactory. In practical applications, physical access to DTACRs may be subject to structural barriers making the collection of thermographic images more complicated. According to the previous process, this can make it difficult or even impossible to perform the analysis using the twelve images. In these cases, a more simplified analysis may be necessary and crucial. Thus, considering the possibility

TABLE 7. Total losses considering a single thermal image.

| Image | Prototype 1 | | | Prototype 2 | | | Prototype 3 | | |
	Temp. (°C)	Losses (W)	Error %	Temp. (°C)	Losses (W)	Error %	Temp. (°C)	Losses (W)	Error %
1	102.0	349.3	1.9	100.3	358.3	2.0	100.7	362.7	1.3
2	101.6	347.4	1.3	100.4	358.8	2.1	100.5	361.9	1.1
3	101.2	345.9	0.9	100.0	356.9	1.6	100.5	361.6	1.0
4	101.1	345.3	0.7	99.6	355.1	1.1	100.6	362.4	1.2
5	101.3	346.1	0.9	100.0	356.9	1.6	100.6	362.3	1.2
6	101.5	347.1	1.2	99.6	355.1	1.1	100.4	361.3	0.9
7	101.5	347.2	1.3	99.4	354.2	0.8	100.3	360.9	0.8
8	101.8	348.3	1.6	99.7	355.6	1.2	101.0	364.1	1.7
9	101.5	347.1	1.2	99.8	356.0	1.3	100.9	363.8	1.6
10	100.8	343.7	0.2	99.6	355.1	1.1	100.6	362.2	1.2
11	100.9	344.4	0.5	99.2	353.3	0.5	100.3	360.6	0.7
12	102.1	349.8	2.0	99.3	353.8	0.7	100.4	361.3	0.9
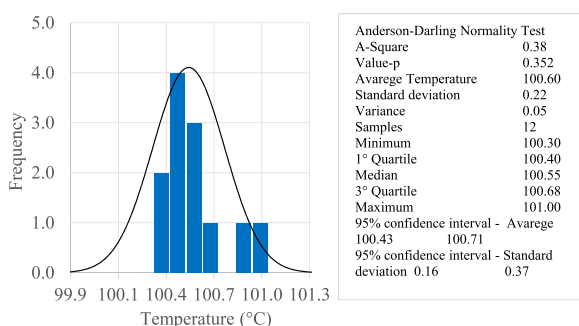
FIGURE 14. Normality test, Prototype 3.

of using a single thermographic image of the prototype to obtain the total losses dissipated, Table 7 was generated to demonstrate the results.

The relative errors (%) of losses compared to the values obtained through measured losses also showed satisfactory values in comparison to the total losses exposed in Table 5. That is, when using a single thermographic image associated with the calorimetric method, a maximum margin of error of 2.1% was found in Prototype 2. So, for restricted cases where the equipment's configuration and arrangement allow us to gather a few thermographic images, the technique can still prove useful.

VII. CONCLUSION

The article presented a proposal for the measurement of the total losses of DTACR with a single coil based on infrared thermography. Results from standard measurement of losses and those obtained from the proposed calorimetric method applied to prototypes showed little difference, even when proposed approximations were considered. From the results, it was also possible to conclude that the constructive differences regarding to the number of layers has practically no influence on the measurement of total losses by the proposed method. It is understood that the calorimetric method can be used in a practical and concise way in order to measure total losses in the winding of DTACRs with a single cylinder. The proposed method is very suitable because thermo images are taken only on the external surface of the reactor, allowing its application in confined spaces. In the same line of reasoning, this article opens up opportunities for the

developments of new studies on DTACR with other constructional characteristics.

REFERENCES

[1] J. C. Das, "Analysis and control of large-shunt-capacitor-bank switching transients," *IEEE Trans. Ind. Appl.*, vol. 41, no. 6, pp. 1444–1451, Dec. 2005.

[2] Y. Varetsky and M. Gajdzica, "Energizing arc furnace transformer in power grid involving harmonic filter installation," *Electr. Rev.*, vol. 4, pp. 64–69, Jan. 2015.

[3] Z. Zhao, P. Fei, S. Bao, and Y. Ding, "Power quality improvement with SVC in power supply system," in *Proc. China Int. Conf. Electr. Distrib.*, Shanghai, China, Sep. 2012, pp. 1–4.

[4] C. Liu, Y. Wu, Y. Su, Y. Wei, B. Shi, and S. Lai, "66 kV phase-controlled reactor fault analysis," in *Proc. China Int. Conf. Electr. Distrib. (CICED)*, Tianjin, China, Sep. 2018, pp. 1293–1296.

[5] S. B. Dalal, W. Knuth, A. Gaun, and A. Grisenti, "Fault current mitigation using 550 kV air core reactors," in *Proc. IEEE/PES Transmiss. Distrib. Conf. Expo. (T&D)*, Denver, CO, USA, Apr. 2018, pp. 1–9.

[6] M. Enohnyaket and J. Ekman, "Analysis of air-core reactors from DC to very high frequencies using PEEC models," *IEEE Trans. Power Del.*, vol. 24, no. 2, pp. 719–729, Apr. 2009.

[7] Y. Zhuang and Y. Wang, "A monitoring method of inter-turn insulation fault for dry-type air-core shunt reactor," in *Proc. 12th Int. Conf. Properties Appl. Dielectric Mater. (ICPADM)*, Xi'an, China, May 2018, pp. 700–703.

[8] L. Hao, J. Zhidong, and W. Xilin, "Study on the mechanism of water infiltrating the package of dry-type air-core," in *Proc. 12th Int. Conf. Properties Appl. Dielectric Mater. (ICPADM)*, Xi'an, China, May 2018, pp. 534–537.

[9] H. Nie, X. Liu, Y. Wang, Y. Yao, Z. Gu, and C. Zhang, "Breaking overvoltage of dry-type air-core shunt reactors and its cumulative effect on the interturn insulation," *IEEE Access*, vol. 7, pp. 55707–55720, 2019.

[10] W. do Couto Boaventura, "Improving the failure detection in the lightning impulse test of low inductance air core reactors," in *Proc. 11th Int. Symp. High-Voltage Eng. (ISH)*, London, U.K., Aug. 1999, pp. 217–221.

[11] H. Shangxi and Z. Minlin, "Energy saved dry-type semi-core reactor," in *Proc. 18th Int. Conf. Exhib. Electr. Distrib. (CIRED)*, Turin, Italy, Jun. 2005, pp. 1–5.

[12] B. S. Ram, "Inductance and winding eddy loss of air-cored reactors," *IEE Proc. Gener., Transmiss. Distrib.*, vol. 146, no. 5, pp. 416–420, Sep. 1999.

[13] T. Ibuchi and T. Funaki, "A study on copper loss minimization of air-core reactor for high frequency switching power converter," in *Proc. 4th IEEE Int. Symp. Power Electron. Distrib. Gener. Syst. (PEDG)*, Rogers, AR, USA, Jul. 2013, pp. 1–5.

[14] X. Nan and C. R. Sullivan, "Simplified high-accuracy calculation of eddy-current loss in round-wire windings," in *Proc. IEEE 35th Annu. Power Electron. Spec. Conf.*, Aachen, Germany, Jun. 2004, pp. 873–879.

[15] M. Enohnyaket and J. Ekman, "PEEC models for air-core reactors modeling skin and proximity effects," in *Proc. IEEE Power Electron. Spec. Conf.*, Orlando, FL, USA, Jun. 2007, pp. 3034–3038.

[16] A. D. Podoltsev, I. N. Kucheryavaya, and B. B. Lebedev, "Analysis of effective resistance and eddy-current losses in multiturn winding of high-frequency magnetic components," *IEEE Trans. Magn.*, vol. 39, no. 1, pp. 539–548, Jan. 2003.

[17] J. Fan and S. Borlase, "The evolution of distribution," *IEEE Power Energy Mag.*, vol. 7, no. 2, pp. 63–68, Mar./Apr. 2009.

[18] G. He, J. Chen, Y. Li, D. Shi, Z. Yang, and J. Wang, "Topology evolution of AC–DC distribution network," in *Proc. IEEE Power Energy Soc. Gen. Meeting (PESGM)*, Atlanta, GA, USA, Aug. 2019, pp. 1–5.

[19] D. Ilisiu and E.-D. Dinu, "Modern reactive power compensation for smart electrical grids," in *Proc. 22nd Int. Conf. Control Syst. Comput. Sci. (CSCS)*, Bucharest, Romania, May 2019, pp. 353–357.

[20] J. H. Harlow, *Electric Power Transformer Engineering*. Boca Raton, FL, USA: CRC Press, 2003.

[21] C. Zhang, Y. Zhao, and X. Ma, "Optimization design of separated dry-type air-core reactor based on modified differential evolution algorithm," in *Proc. IEEE 3rd Int. Conf. Inf. Sci. Technol. (ICIST)*, Yangzhou, China, Mar. 2013.

[22] Z. Han, L. Zou, H. Song, L. Zhang, T. Zhao, and Y. Sun, "Study on optimal structure of three-loop simplified scaling model for dry-type air-core reactors," *IEEE Access*, vol. 6, pp. 48259–48267, 2018.

[23] M. F. Khan, A. L. L. Jarvis, E. A. Young, A. G. Swanson, J. C. Archer, and R. G. Stephen, "Design, construction, and testing of a desktop superconducting series reactor toward the grid installation of a prototype unit," *IEEE Trans. Appl. Supercond.*, vol. 30, no. 5, pp. 1–6, Aug. 2020.

[24] F. Chu, Y. Fu, Q. Wang, X. Wu, Z. Liu, and X. Lei, "Analysis of static magnetic flux density and electromagnetic force distribution of a dry-type air-core reactor under different operating current," in *Proc. 22nd Int. Conf. Electr. Mach. Syst. (ICEMS)*, Harbin, China, Aug. 2019, pp. 1–4.

[25] F. Yuan *et al.*, "Thermal optimization for dry type air core reactor base on FEM," in *Proc. 21st Int. Conf. Electr. Mach. Syst. (ICEMS)*, Jeju, South Korea, Oct. 2018, pp. 1726–1730.

[26] A. S. Antonov and D. A. Glushkov, "Research on electromagnetic and heat processes in dry type air core current-limiting reactors," in *Proc. IEEE Conf. Russian Young Researchers Electr. Electron. Eng. (EIConRus)*, St. Petersburg, Russia, 2017, pp. 1471–1476.

[27] F. Chen, Y. Zhao, and X. Ma, "An efficient calculation for the temperature of dry air-core reactor based on coupled multi-physics model," in *Proc. 6th Int. Conf. Electromagn. Field Problems Appl.*, Jeju, South Korea, Jun. 2012, pp. 1–4.

[28] F. T. Yuan, Z. Yuan, J. X. Liu, Y. Wang, W. X. Mo, and J. J. He, "Research on temperature field simulation of dry type air core reactor," in *Proc. 20th Int. Conf. Electr. Mach. Syst. (ICEMS)*, Sydney, NSW, Australia, Aug. 2017, pp. 1–5.

[29] *Power Transformers Part 6—Reactors, International Electrotechnical Commission*, document IEC-60076-6, 2013.

[30] *IEEE Guide for the Application of Shunt Reactor Switching*, IEEE Standard C37.015 TM, 2009.

[31] *Requirements, Terminology, and Test Code for Dry-Type Air-Core Series-Connected Reactors*, IEEE Standard C57.16 TM, 2011.

[32] *IEEE Standards for requirements Terminology, and Teste Code for Dry-Type Air-Core Series-Connected Reactors*, IEEE Standard C57-2011, Feb. 2012.

[33] O. Osemwinyen, S. B. Shah, and A. Arkkio, "Thermographic method for measuring iron losses and localized loss density," in *Proc. 7th Int. Electr. Drives Prod. Conf. (EDPC)*, Würzburg, Germany, Dec. 2017, pp. 1–4.

[34] H. Shimoji, B. E. Borkowski, T. Todaka, and M. Enokizono, "Measurement of core-loss distribution using thermography," *IEEE Trans. Magn.*, vol. 47, no. 10, pp. 4372–4375, Oct. 2011.

[35] E. C. Bortoni, R. A. Yamachita, J. M. C. Guimaraes, and M. C. C. Santos, "Losses estimation in induction motors using infrared thermography techniques," in *Proc. 12th Int. Conf. Quant. Infr. Thermography*, Bordeaux, France, Jan. 2014, pp. 1–8.

[36] E. da Costa Bortoni, R. T. Siniscalchi, and J. A. Jardini, "Determination of hydro generator efficiency using infrared thermal imaging techniques," *IEEE Trans. Energy Convers.*, vol. 26, no. 4, pp. 1134–1139, Dec. 2011.

[37] E. da Costa Bortoni and R. T. Siniscalchi, "Hydro generators losses measurement in accordance to IEEE-STD-115 and IEC-60034-2," in *Proc. IEEE Power Energy Soc. Gen. Meeting*, San Diego, CA, USA, Jul. 2012, pp. 1–6.

[38] E. C. Bortoni, R. A. Yamachita, F. M. Silva, and D. G. Mesquita, "Distribution transformer efficiency measurement using infrared thermography," in *Proc. 14th Quant. Infr. Thermography Conf.*, Berlin, Germany, 2018.

[39] H. D. Young and R. A. Freedman, *Physics III: Electromagnetism*. 12th ed. São Paulo, Brazil: Pearson, 2009.

[40] T. L. Bergman, A. S. Lavine, F. P. Incropera, and D. P. DeWitt, *Fundamentals of Heat and Mass Transfer*, 8th ed. Hoboken, NJ, USA: Wiley, 2017.

[41] C. H. Forsberg, *Heat Transfer Principles and Applications*. New York, NY, USA: Academic, 2020.

[42] B. W. Martin, "Free convection in a vertical cylinder with internal heat generation," *Proc. Roy. Soc. London A, Math. Phys. Sci.*, vol. 301, pp. 327–341, Oct. 1967.

[43] H. Kaplan, "Practical applications of infrared thermal sensing and imaging equipment," in *Tutorial Texts in Optical Engineering*, 3rd ed. Bellingham, WA, USA: SPIE, 2007.

[44] M. Litwa, "Influence of angle of view on temperature measurements using thermovision camera," *IEEE Sensors J.*, vol. 10, no. 10, pp. 1552–1554, Oct. 2010.

[45] P. R. Muniz, S. P. N. Cani, and R. D. S. Magalhaes, "Influence of field of view of thermal imagers and angle of view on temperature measurements by infrared thermovision," *IEEE Sensors J.*, vol. 14, no. 3, pp. 729–733, Mar. 2014.

[46] D. C. Montgomery and G. C. Runger, *Applied Statistics and Probability for Engineers*, 7th ed. Hoboken, NJ, USA: Wiley, 2018.

DENISON GIMENES MESQUITA (Student Member, IEEE) was born in Itajubá, Brazil, in May 1980. He received the bachelor's and master's degrees in electrical engineering from the Federal University of Itajubá (UNIFEI), Itajubá, in 2007 and 2020, respectively. He worked at Alstom for two years as a Project Engineer of dry-type air-core reactors, where he was an Engineering Supervisor. At General Electric (GE), Itajubá, he was responsible of high voltage laboratory, where main activities were to supervise routine and type tests in dry-type air-core reactors and power capacitors, in addition to participating in high voltage laboratory project team. He is a Researcher at EXCEN and the Excellence Center in Energy Efficiency. He is a Student Member of IEEE Power and Energy Society.

EDSON DA COSTA BORTONI (Senior Member, IEEE) was born in Maringá, Brazil. He received the bachelor's degree in electrical engineering from the Federal University of Itajubá (UNIFEI), Itajubá, Brazil, in 1990, the M.Sc. degree in energy systems planning from the University of Campinas, Campinas, Brazil, in 1993, the D.Sc. degree in power systems from the Polytechnic School, University of São Paulo (USP), São Paulo, Brazil, in 1998, and the Habilitation degree from USP, in 2012. He is currently a Professor at UNIFEI and its present rector. He is also the Head of the EXCEN, the Energy Efficiency and Renewable Generation Excellence Center. His research interests include electrical machines design and modeling, sensors, power generation, smart grids, and energy systems development. He is a Fellow Member of International Hydropower Association and the International Society of Automation. He is a Distinguished Lecturer of IEEE, the Secretary of the EMC, an Assistant Editor and Subject Editor of IET GTD, and an Assistant Editor of the *Flow Measurement and Instrumentation* and the IEEE Transactions on Energy Conversion.

DAVI MARCELO FÉBBA (Student Member, IEEE) was born in Vilhena, Brazil, in April 1992. He received the B.Sc. degree in physics and the M.Sc. degree in physics (condensed matter) from the Federal University of Itajubá (UNIFEI), Itajubá, Brazil, in 2016 and 2018, respectively, where he is currently pursuing the Ph.D. degree in electrical engineering. He works with applied statistics and the effects of temperature and irradiance on solar cells electrical parameters, and the influences of noise on metaheuristic algorithms applied to the photovoltaic parameter extraction problem.

ROBERTO TEIXEIRA SINISCALCHI (Senior Member, IEEE) was born in Itajubá, Brazil, in January 1967. He received the B.S. degree in electrical engineering and the M.Sc. degree in energy engineering from UNIFEI in 1993 and 2009, respectively, and the M.B.A. degree from Cândido Mendes (UCAM). He is currently with Furnas Centrais Elétricas, where he is responsible for the operation of three hydro power plants totaling 2872 MW, ten power substations, and about the 3000 km of transmission lines in 345 and 500 kV. His research interests include maintenance, field testing, and power generation.